π-PIC: a framework for modular particle-in-cell developments and simulations

Frida Brogren, Christoffer Olofsson, Joel Magnusson, and Arkady Gonoskov

Department of Physics, University of Gothenburg, SE-41296 Gothenburg, Sweden

November 14, 2025

Abstract

Recently proposed modifications of the standard particle-in-cell (PIC) method resolve long-standing limitations such as exact preservation of physically conserved quantities and unbiased ensemble down-sampling. Such advances pave the way for next-generation PIC codes capable of using lower resolution and fewer particles per cell, enabling interactive studies on personal computers and facilitating large-scale parameter scans on supercomputers. Here, we present a Python-controlled framework designed to stimulate the dissemination and adoption of novel PIC developments by providing unified interfaces for accommodation, cross-testing, and comparison of PIC solvers and extensions written in Python or low-level languages like C++ and Fortran. To demonstrate flexibility of proposed interfaces we present and test implementations of several PIC solvers, as well as of extensions that is capable of managing QED processes, moving-window, and tight focusing of laser pulses.

1 Introduction

In recent years, impressive progress has been made in developing advanced particle-in-cell (PIC) schemes that overcome, or mitigate, fundamental limitations of this method. Significant effort has been dedicated to creating faster, more versatile, exact and user-friendly PIC codes. Some of the most well-used codes includes (but are not restricted to) PIConGPU [1], Smilei [2], Epoch, Osiris [3], PICADOR [4] and the codes included in the BLAST project (e.g. WarpX [5], WakeT, HiPACE and FBPIC [6]). Codes, like Smilei, Osiris, Epoch and WarpX are targeting a wide user base with a large variety of functionality suitable for different types of interactions, for example ionization, Breit-Wheeler pair creation and radiation reactions, ionization, Schwinger process and collisions. Other codes, including FBPIC, WakeT, and HiPACE, aim to enhance speed through different strategies, such as employing simplified geometries, adopting quasi-static methods, and utilizing boosted frame simulations.

Despite these advances, as the PIC community grows and the applicability of PIC codes enlarges the need for testing and incorporating new physics and algorithms persists. At the same time, as these codes evolve, several with focus on optimized execution, modifying them becomes more complex and expensive from a developers perspective. In other areas of computational physics and applied mathematics, such challenges have been alleviated by standard interfaces that enable testing and comparison of different methods within a single design pattern (see, e.g. OpenFOAM [7], ASE [8], LAMMPS [9], BLAS [10], LAPACK [11], FFTW [12], COIN-OR [13] and Scikit-learn [14]).

Certainly, the developers of almost every well-established PIC code strive to cover such functionality, but for the wider PIC community, such interface remains to be established. Three distinct difficulties can be identified. The first is related to compatibility of physical units, design patterns and interfaces that vary across codes and communities. In particular, performance is often prioritized over flexibility and simplicity, while these aspects appear to be crucial for cross-community efforts. The second difficulty is centralization of developments: even in the case of open-source development using GitHub or other platforms, in practice any contribution of a significantly new scheme requires setting up a collaboration with the lead developers, which can slow down testing unestablished novel ideas. The third difficulty is the necessity of contributors to have profound knowledge of the programming language chosen for the project.

In this paper we report on our experience of developing an interface that appears to overcome these obstacles. Compatibility is addressed by a framework that supports a variety of solvers and extensions,

which can be implemented in C++, Fortran or any other language that provide callable functions and, thereby, does not compromise efficiency. Multithreading can be used directly within this setup, while GPU and multi-node execution require additional development, which, however does not appear to face any fundamental obstacles. The approach is decentralized: new solvers and extensions can be developed completely independently and coupled within Python. The capabilities of the devised interface are shown by considering a number of solvers, practical extensions and Python scripts that combine them for performing validation tests.

The paper is arranged as follows: in section 2, we give a brief overview of selected PIC algorithms, numerical inaccuracies connected to the methods and future prospects. Section 3 considers architecture and utilization of the presented framework called π-PIC. Section 4 presents extensions for beam-plasma interaction and in section 5.1 the development and testing of an electrostatic solver. To further demonstrate opportunities for incorporating non-conventional solvers in section section 5.2 we describe an explicit, relativistic PIC solver, called emc2, that preserves energy and has improved properties with respect to momentum conservation. In section 5.3, we show benchmark of a energy-conserving solver [15] implemented in π-PIC against Smilei [2] in the context of laser-wakefield acceleration.

2 Limitations and prospects for the PIC method

The challenges of simulating plasma typically revolve around reducing numerical artifacts or increasing computational efficiency. This section begins with a brief overview of the fundamentals of the PIC algorithm, then turns to a discussion of various solvers, their role in mitigating or damping numerical artifacts and instabilities, and the implications these choices have for computational performance.

The PIC algorithm is normally divided into four steps: (1) particle push, where the particles are advanced using the Lorentz equation, (2) charge deposition, where the particle position and momentum are used to calculate current and densities, (3) field advancement, where the electromagnetic field is advanced and (4) field gathering, where the field is interpolated back to the particle position. Important variations of this scheme includes the type of charge deposition, choice of field solver, macro-particle shape function and particle push.

Methods are typically grouped into relativistic or non-relativistic and electrostatic or electromagnetic. Deciding whether to use relativistic or non-relativistic and electrostatic or electromagnetic codes largely depends on the plasma state being simulated and the governing physics. Additionally, methods can be classified based on their implementation as implicit, explicit, spectral, global and local. Implicit methods evolve some physical state by solving a system of equations, usually in the form of a matrix equation, an operation which often is done iteratively. In contrast, explicit methods advance the state using only the current state and past states of the system. On the other hand, spectral methods are based on an explicit field advancement in Fourier space representation. Global methods employs a global calculation to advance the state while local methods only uses the state of the current and neighboring nodes. Spectral methods are inherently global due to the Fourier transform, while explicit and implicit methods can be either local or global. More generally, PIC algorithms can use global or local and implicit or explicit routines, using coordinate or spectral representation in different parts of the algorithm.

Due to their parallelization capability and fast execution, explicit local methods typically achieve higher computational speeds than other approaches. Moreover, the rapid growth of parallel computing resources has driven a broad preference for explicit methods. However, generally, these methods are less stable compared to implicit (or spectral) methods which can allow larger time step and better conservation of important quantities like energy and charge. Typically, numerical artifacts stem from inaccuracies in numerical schemes which changes the dynamics of the system and leads to an accumulation of errors manifesting as a violation in the laws of physics. In the following we examine three examples of this, highlighting the trade-off between accuracy and computational speed: (1) numerical dispersion, (2) charge accumulation, and (3) momentum and energy non-conservation.

Numerical dispersion emerges as a result of the discretization of electromagnetic waves, causing the discretized waves to travel at velocities that differ from the speed of light. A popular choice of Maxwell solver is Finite-Difference Time-Domain (FDTD) [16] which shows direction-dependent numerical dispersion. Suggestion for a modified FDTD schemes which mitigates numerical dispersion completely in some directions and partly in others came in 1999 [17] and since then more have followed [18–21]. Setting aside FDTD maxwell-solver, numerical dispersion can be entirely avoided by using a spectral solver [22] which solves the spatial part of maxwells equations in Fourier space and advances the field in the time-domain. However, this is done at the expense of doing a global Fourier transform operation. For this reason, finite-difference methods was long preferred over spectral solvers. Yet, in 2013 a parallelized implementa-

tion using domain decomposition was presented in [23] and has since then been popularized and further developed in codes such as WarpX [5] and FBPIC [6].

Apart from low numerical dispersion other desirable properties of PIC codes are charge conservation. Charge conservation is equivalent to fulfilling the continuity equation. Ampères-Maxwells law is used to advance the field in time, however, Gauss's law is not included, as it does not depict the evolution of the state. Consequently, one tactic to ensure charge conservation is by correcting the fields retroactively using Gauss law [22, 24, 25]. Another option is to adopt a so called current deposition scheme that ensures current conservation locally [26–30]. Again, the second options has some benefits as it is a local operation while the correction of Gauss law must be carried out globally.

Furthermore, the PIC scheme in its standard implementation does not conserve energy nor momentum. This may result in numerical heating, in particular if the Debye length is not resolved aliased modes will appear as thermal fluctuations [31–33]. One method to address this is employing smoother shape functions, acting as a low-pass filter for small wavelength oscillations [22], essentially reducing spatial invariance thereby achieving better momentum conservation. Another way to limit numerical heating is to employ energy conserving schemes. In general these are constructed using an implicit solver [34]. π-PIC however comes equipped with an explicit energy conserving (`ec` and `ec2`) solver [15]. Another promising approach for achieving energy conservation has been recently proposed by Rickertson and Hu in [35] and demonstrated for the case of non-relativistic PIC simulations.

The preceding discussion indicates a connection between the accumulation of numerical artifacts and the failure of numerical methods to comply with conservation laws. Unsurprisingly, a discretization of a continuous theory with a set of symmetries and associated conservation laws, does not automatically inherent these symmetries. However, in the past decade a new research area for the design of PIC codes which inherently respect conservation laws has emerged. So called structure-preserving codes [36] uses geometric integrators to achieved exact charge conservation by building algorithms based on principles of gauge invariance [37, 38]. Similar techniques can also provide energy conservation [39]. We consider this line of research a good prospect for further development of the PIC algorithm.

To summarize, a diverse range of PIC implementations is currently available. To further advance the field, it is necessary to develop a unified platform where different code variations can be tested, compared and studied to reveal their preferable domains of use. The objective of π-PIC is to support a wide range of diverse solvers, while ensuring they remain compatible with extensions that enable additional functionalities, such as ionization injection, radiation reaction and strong-field QED [40, 41], as well as ensemble downsampling [42, 43].

3 The π-PIC framework

To accommodate maximum freedom for the user, the π-PIC framework offers three interaction levels that can be used to modify the code: (1) the Python interface, (2) extensions and (3) solvers.

The first, entry level, offers functionality for initializing the simulation with arbitrary fields and particle densities as well as advancing the system state, see fig. 1. Additionally, it provides runtime read capabilities for particle phase-space, and both runtime read and modification access of fields. The PIC algorithm itself is written in C++ and the linking between Python and C++ is realized using pybind11 [44]. Custom functions, defined in the Python interface used to preform actions on the simulation state, are compiled from Python into C++ code using the Numba decorator `@cfunc()`. The decorator indicates parts of the code that are precompiled to avoid a potential loss of efficiency in performance-critical parts. There are three types of predefined decorator functions available in π-PIC: `add_particle_callback`, `field_loop_callback` and `particle_loop_callback`. Each of these callbacks accepts a predefined set of arguments (such as particle position, weight, and electric field), which are described in the example script (section 4).

The final two arguments of every π-PIC callback, `data_double` and `data_int`, correspond to C++ pointers referencing a float64 array and an int32, respectively. These can be used to pass memory addresses for storing or retrieving data (see fig. 1). For instance, one might supply the address of a Numpy array to which the electric field should be written. This mechanism enables dynamic data exchange between Python and the C++ backend across PIC update steps.

The second interaction level is the extensions, which are added in the Python interface and then attached to each execution in connection to each PIC update. Extensions can be written in Python or in C++ and provides a handle for further modification of particle state as well as field state. This is particularly useful for developing, for example, new ionization routines or incorporating collisional

and strong-field effects. The development and application of extensions are further discussed and exemplified in section 4. The extensions are added to the advance routine in the Python interface by the `add_handler()` call, see fig. 1.(L:8). This places the defined handlers in a list in the `handlerManager` which is then called during each advance call of the simulation. A step-by-step tutorial on how to develop and employ an extension can be found at [45].

The final interaction level is dedicated to the employment of new solvers. In π-PIC solvers are composed of two defining classes: A `pic_solver` and a `field_solver` that specifies the advancement of particle states and fields respectively. The `field_solver` is a mandatory member of the `pic_solver` class, reflecting the fact that field and particle updates are generally coupled and must be advanced consistently. This composition enforces a clear ownership hierarchy: the `pic_solver` manages the `field_solver`. Developers may still implement or replace individual components (e.g. particle pusher) while reusing an existing `field_solver` or `pic_solver`. Furthermore, this class structure allows for a large degree of freedom in terms of the implementation of the PIC update, for example, part of the field update can be done concurrently with the particle update, as is the case for the energy conserving (EC) solver [15] implemented in π-PIC.

To maintain compatibility with the rest of the framework, there is a number of mandatory and optional class methods that every `field_solver` and `pic_solver` implements. These are defined in the header file named `interfaces.h`. Provided that the new solver follows the same structure as the template, it will be compatible with all previously developed extensions.

With the flexibility granted by this framework, the only fundamental limitation imposed on the developer is that particles are stored in the `CellInterface` on a cell-by-cell basis. This ensures that extensions can access particles efficiently. Fields, in contrast, are accessed by extension through the `field_solver`, allowing developers to define and update them according to their needs. This enables support for staggered grids and non-Cartesian geometries. In section 5 we will further describe the implementation of solvers by the example of an electrostatic solver, as well as testing the accuracy of solvers in simulating Laser Wakefield acceleration.

4 Extensions

In this section, we describe the role of extensions in π-PIC, along with some of the extensions, useful for laser-plasma interaction, that have already been implemented. Extensions provide functionality for modifications of particles and fields which can be applied on top of the chosen PIC solver.

To access particles and fields during the `advance` call extensions has two defining methods: a `handler`, for modifying, adding and removing particles, and a `fieldHandler` for modifying fields. The input arguments to the handler `handler` is repacked into a `cellInterface` for easy access to cell data, such as fields, cell dimension, cell node position, number of particles and particle buffer size. At the advance call, the `ensemble` loops over the existing cells in a multi-threaded process, applying the action of `handler`. In `handler` particles can be removed by setting their weight to zero and added by writing to the particle buffer. Additionally, the particle momentum can be arbitrarily modified, however, the position should be changed with care, since particle migration to other cells can cause the particle buffer to overflow. The `fieldHandler` has input arguments, such as field, position and index. As for the `handler` the `fieldHandler` method is applied at the advance call to all points in the field grid. It is, however, the `fieldSolver` which defines how the loop is executed, enabling different types of grid geometries and staggering.

Here we present two extensions which utilizes both the `handler` and `fieldHandler`: an implementation of absorbing boundaries with replacement of particles (section 4.1) and a moving window (section 4.2). Additionally, we present an extension for mapping a spatially extended pulse to its focus (section 4.3).

4.1 Absorbing boundaries

Periodic and absorbing (or open) boundary conditions are arguably the most common choice in plasma simulations. Generally, implementing periodic boundary conditions is straightforward, as it mainly involves linking the ends of the simulation box. Free boundary conditions are more challenging, as it theoretically implies placing the boundary at infinity or restricting the type of electro-magnetic waves allowed at the boundary - namely no incoming waves. For this reason, open boundary conditions are most commonly emulated by introducing an absorbing medium at the boundary. A popular implementation is Perfectly Matched Layers (PML) [46], where, so called, complex coordinate stretching is used to emulate

```
1:  sim=pipic.init(solver='solver',...)

2:  @cfunc(types.add_particles_callback)
    def density_profile(r,...):
        return density
3:  sim.add_particles(name='particle_name',
                      density=density_profile.address,...)

4:  @cfunc(types.field_loop_callback)
    def initialize_field(ind, r, E, B,...):
        # Initialize field
5:  sim.field_loop(handler=initialize_field.adress,...)

6:  @cfunc(types.particle_loop_callback)
    def particle_callback(r, p, w, data_double,...):
        # Save particle momentum/position

7:  @cfunc(types.field_loop_callback)
    def field_callback(ind, r, E, B, data_double,...):
        # Modify or save fields

8:  sim.add_handler(subject='particle_name,cells',
                    handler=extension.handler(),...)
    for i in range(simulation_steps):
9:      sim.advance(time_step=time_step, use_omp=True,...)
10:     sim.particle_loop(name='particle_name',
                          handler=particle_callback.address,
                          data_double=pipic.addressof(particle_dd))
11:     sim.field_loop(handler=field_callback.address,
                       data_double=pipic.addressof(field_dd)
                       use_omp=True,...)
```
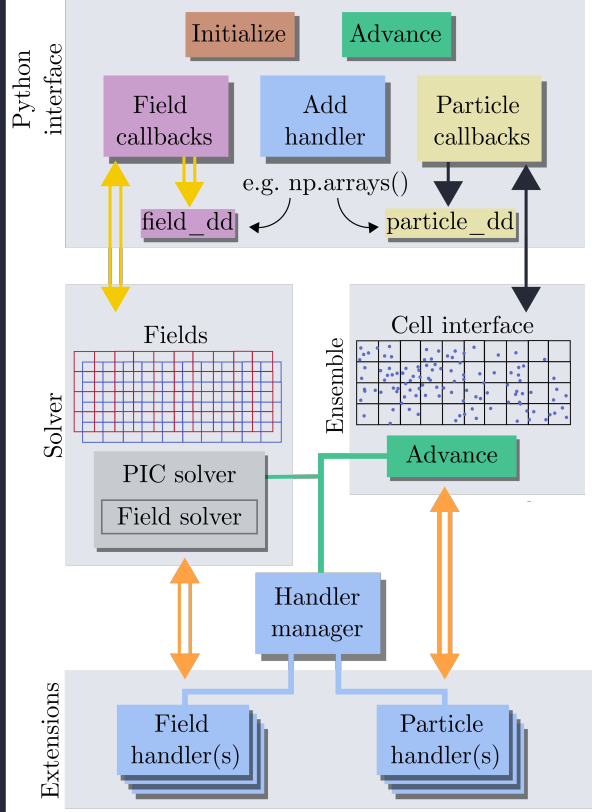
Figure 1: To the left, a simplified main script for simulation with π-PIC is shown, a full version can be seen in section A. Line 1 initiates the simulation instance. Line 2-5 adds particles and fields to the simulation. Line 6-7 defines functions which loops over fields and particles for saving or modification. All predefined decorator functions in the Python interface has a `data_double` and `data_int` as arguments. This allows the user to pass an address to a Numpy array which can be used to record the particle or field state, see line 10-11. Line 8 adds the extension to the advance call. During the advance call (line 9) the extensions and solver are applied to each cell and associated particles in a multi-threaded process. Line 9 advances the simulation state, executing the PIC solver and field solver and added extensions. The `use_omp` key word is used to activate multi-threading. The existence of multi-threaded processes is denoted as double arrow in the right scheme. Line 9 and 10 loops through the particles and field, passing an address to the double arrays `particle_dd` and `field_dd`, respectively, for saving the simulation state. The different instances of the code in the scheme to the right are color coded to match the Python commands that activates them.

an absorbing space within a few grid points. Here, we take on a minimalistic approach known as masking, where incoming electromagnetic fields are gradually depleted by iterative attenuation [47].

For our implementation of free boundary condition the field is attenuated at every iteration by

$$\tilde{E}(x) = R(x)E(x), \quad \tilde{B}(x) = R(x)B(x) \tag{1}$$

where $R(x)$ is the masking function and $\tilde{E}, \tilde{B}$ are the updated fields. To avoid absorption changing with the length of timestep, we require that the cumulative attenuation after n time steps Δt, to be equal to the attenuation obtained using a single time step of size $n\Delta t$, that is $R(x, \Delta t)^n = R(x, n\Delta t)$. This condition is full-filled by the choice

$$R(x, \Delta t) = e^{\Delta t r(x)}. \tag{2}$$

Moreover, to minimize reflection we demand that $r(x_b) = 0$ and $\frac{dr(x_b)}{dx} = 0$, where x_b is the start of the boundary. Additionally we require that $\lim_{x \to x_{\max}} R(x) \to 0$ which gives the condition $\lim_{x \to x_{\max}} r(x) \to -\infty$. A function that satisfies these conditions is

$$r(x_r) = \alpha \left[\cos(\pi x_r/2) - \frac{1}{\cos(\pi x_r/2)} \right], \tag{3}$$

where $x_r = \frac{x-x_b}{x_{\max}-x_b}$ is the relative, normalized position at the boundary such that $x_r \in [0, 1]$ and α is a shape parameter controlling the steepness of the absorption, see fig. 2.(b). We assess the absorption by letting a Gaussian beam with wavelength $\lambda = 1\,\mathrm{cm}$ pulse duration $t_s = 5\,\mathrm{fs}$ and equal transverse extent, propagate at an angle of $45°$ towards the boundary as shown in fig. 2.
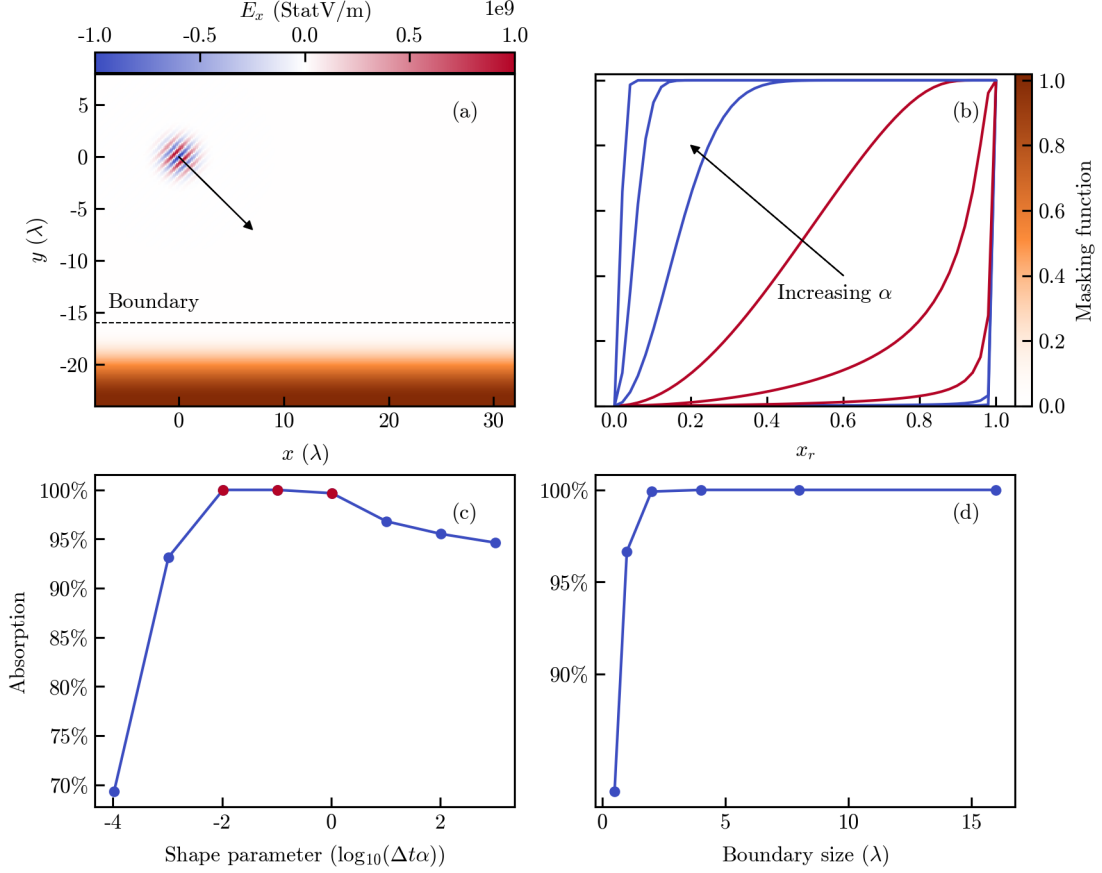

Figure 2: Panel (a) shows the initial field of the simulation: a Gaussian pulse is propagating at $45°$ angle towards the boundary where the masking function $R(y)$ is shown in orange color scale. Panel (b) shows the difference in absorption function with different shape factors α. The red curves corresponds to boundaries with maximal absorption as shown in panel (c). For these simulations the boundary size was set to four wavelengths. Panel (d) shows the dependence of the absorption on boundary size. The shape factor corresponding to $\Delta t \alpha = 1$ was used for these simulations. The absorption was calculated as the decrease in total electromagnetic energy before and after interaction with the boundary.

The disadvantage of this approach, compared to other implementations, such as PMLs, is that it requires a large damping region. Here, we find that a damping region > 4 wavelengths achieves sufficient absorption.

To fully emulate open boundaries in plasma simulations particles needs to be added and removed to maintain a constant density and velocity distribution at the boundary. Similar to fields, this must be done gradually and smoothly to avoid introducing artifacts and high-frequency noise at the boundary. We propose removing particles at the same rate as fields, while simultaneously adding particles with velocity distributions determined by temperature.

Since the primary reason for this work was to showcase the use of extensions to modify fields and particles, no comparative study with other methods has been made. These comparisons, as well as the possible implementation of more advanced methods, are left for future work. The code implementation can be found at [45].

4.2 Moving window

For simulation involving, for example, laser-plasma interaction the computational demands can typically be greatly reduced by only simulating a region of space that moves with the process of interest. For

example, this is the case when simulating a laser pulse or a relativistic bunch of electrons. To achieve this a *moving window* is used.

The available solvers in π-PIC all have spectral field solvers, consequently the default boundary condition is periodic and a propagating field will reappear at the opposite side of the simulation box if it passes through the boundary. This makes the implementation of the moving window rather simple. For a moving window with speed v we need to remove the fields and all plasma perturbation in a region which moves around the simulation box with the same speed. The full implementation and use of the moving window is documented in [45].

4.3 Mapping of tightly focused laser pulses

Tightly focused laser pulses are central to studies of high-intensity laser–matter interactions [48, 49], fundamental quantum systems [50] and various areas of attosecond physics [51]. While analytical methods exist [52–56] to describe the propagation of their associated electromagnetic fields, numerical approaches provide a more direct and flexible alternative, free from the inaccuracies introduced by simplifying assumptions. Such computations are particularly relevant for vacuum electron acceleration [57], and radiation generation driven by laser–electron dynamics, where interactions are highly sensitive to the structure of the focal electromagnetic field [58–60]. However, numerical techniques based on direct integration of Green's functions or FDTD methods can be computationally intensive and prone to numerical dispersion. Spectral field solvers on the other hand, as implemented in π-PIC, leverage fast Fourier transforms to evolve the electromagnetic field. This enables dispersion-free computation of the focal field of tightly focused laser pulses, given a known far-field profile, within a single time step. Despite this advantage, the simulation box Ω_B must be sufficiently large to encompass the initial laser pulse profile. Consequently, excessive computational effort is spent evolving the simulation in regions where no significant dynamics occur, even though the physical interaction of interest is many times confined to a much smaller box $\Omega_b \subseteq \Omega_B$ (see fig. 3). To avoid this computational overhead, the periodic boundary conditions imposed by spectral solvers can be leveraged. In what follows, we further develop the approach proposed in [61]: since the divergence of previously focused radiation defined in a space with cyclic geometry results in overlaying and summing of electromagnetic radiation, one can time reverse this process and obtain a focused radiation by time advancement of summed, overlaid radiation before focusing.

Indeed, any point $\mathbf{r} = (x, y, z)$ inside a given simulation box is equivalent to a point outside the computational domain according to the identification

$$\mathbf{r} \sim \mathbf{r} + \mathbf{L}, \quad \mathbf{L} = (L_x, L_y, L_z), \tag{4}$$

where L_x, L_y and L_z are the simulation box lengths along each coordinate axis, respectively. In other words, any two coordinates that differ by a multiple of the box lengths, represent the same physical point. Moreover, eq. (4) implies that electromagnetic fields initialized in Ω_B admit an equivalent representation within Ω_b. This suggests that the initial pulse can be mapped directly onto Ω_b, after which the electromagnetic field can be evolved over a single time step, thereby avoiding the need to include the full extent of the far-field. To perform such a mapping, a set of coordinates enclosing the initial pulse profile, relative to the simulation box Ω_b must be defined. One approach is to assume that the laser pulse initially occupies a spherical segment with thickness ℓ, aperture angle $\theta_{\max}$, and radius R_0. The latter is interpreted as the distance from the pulse centroid to the location of the focus. Then, letting $i, j, k \in \mathbb{Z}$ denote integer steps that constitutes the box Ω_b, the electric (and magnetic) field at any location in Ω_b can be written as

$$\mathbf{E}\left(i\Delta x, j\Delta y, k\Delta z\right) = \sum_{h_x=h_x^-}^{h_x=h_x^+} \sum_{h_y=h_y^-}^{h_y=h_y^+} \sum_{h_z=h_z^-}^{h_z=h_z^+} \mathbf{E}\left([h_x n_x + i]\,\Delta x,\ [h_y n_y + j]\,\Delta y,\ [h_z n_z + k]\,\Delta z\right), \tag{5}$$

where $\Delta x, \Delta y, \Delta z$ and n_x, n_y, n_z are the spatial resolution and number of cells along each coordinate axes of Ω_b, respectively. Here, the integers h_m with $m \in \{x, y, z\}$ are referred to as *hypercells*, which are periodic replicas of Ω_b arranged to fully enclose the initial pulse profile. The hypercell bound for each coordinate axis is given by

$$h_m^{\pm} = \left\lfloor \frac{L_m/2 \pm (R_0 + \ell/2)}{L_m} \right\rfloor. \tag{6}$$

An example of Ω_b is depicted in fig. 3(a) as the shaded quadratic region, whereas the three bottom rows of unshaded squares demarcate the required hypercells to accurately capture the pulse profile. To avoid
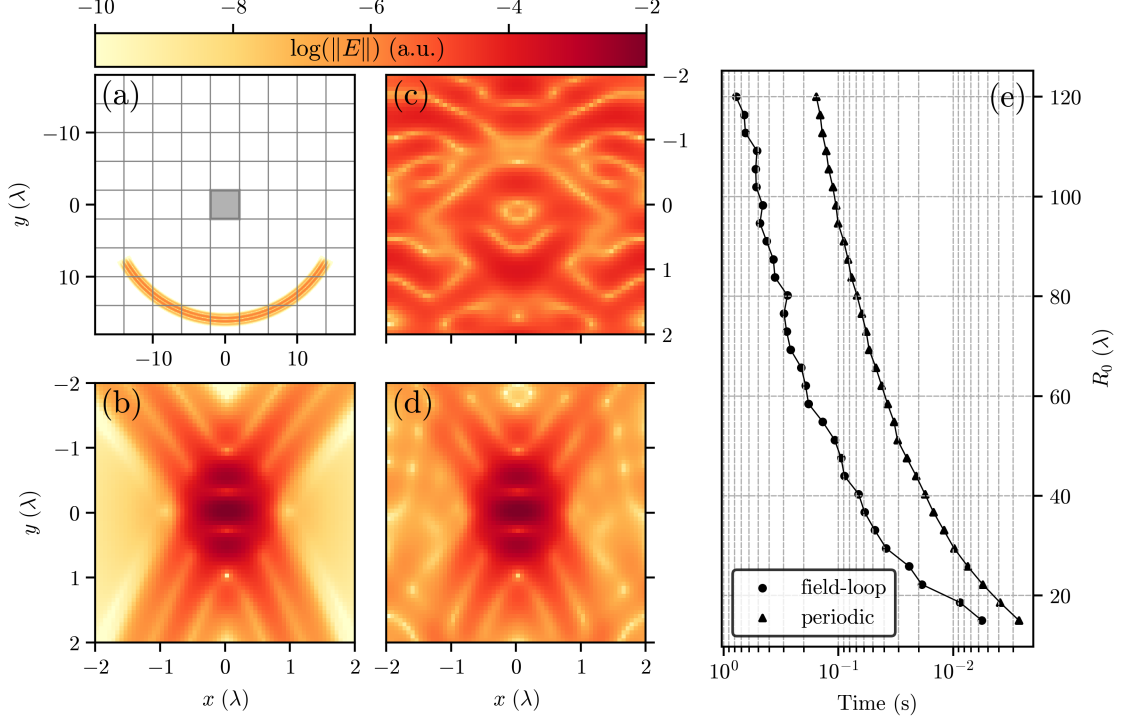
Figure 3: Electric field strength of the initial laser pulse after initialization within (a) Ω_B and (c) Ω_b, along with the corresponding field states after a time step R_0/c shown in (b) and (d), respectively. In (a), the shaded gray square indicates the extent of Ω_b, while the surrounding unshaded squares represent equivalent coordinates within Ω_B. Panel (e) shows the average runtime across 15 runs for the initialization and propagation of the electromagnetic fields as a function of R_0.

superimposing negligible electromagnetic fields, arising from e.g. empty cells, only the coordinates that satisfy

$$|R_0 - r| \le \frac{\ell}{2}, \quad \theta = \arccos(\hat{r} \cdot \hat{n}) \le \theta_{\max}, \tag{7}$$

are included. Here, $r = |\mathbf{r}|$, $\hat{r} = \mathbf{r}/r$, and $\hat{n}$ is the unit vector along the direction of R_0. The specific implementation of the periodic mapping, including an optimized procedure, is provided in [45], and is demonstrated next.

To demonstrate the periodic mapping, we perform 2D simulations for a linearly polarized focused pulse with central wavelength λ. We take the axis of propagation to be along y, using a dimensionless far-field pulse profile u analogous to that given in [61]:

$$u(\mathbf{r}) = \frac{u_\parallel(r - R_0)}{r} u_\perp(\theta), \tag{8}$$

where

$$u_\parallel(\xi) = \sin\left(\frac{2\pi\xi}{\lambda}\right) \cos^2\left(\frac{\pi\xi}{\ell}\right) \Pi\left(\xi, -\frac{\ell}{2}, \frac{\ell}{2}\right), \tag{9}$$

is the longitudinal profile and $\Pi(\xi, \xi_{\min}, \xi_{\max})$ is the rectangular function that equals unity whenever $\xi \in [\xi_{\min}, \xi_{\max}]$ and zero otherwise. The transverse shape is given by

$$u_\perp(\theta) = \Pi\left(\theta, 0, \theta_{\max} - \frac{\varepsilon}{2}\right) + \cos^2\left(\frac{\pi\left(\theta - \theta_{\max} + \frac{\varepsilon}{2}\right)}{2\varepsilon}\right) \Pi\left(\theta, \theta_{\max} - \frac{\varepsilon}{2}, \theta_{\max} + \frac{\varepsilon}{2}\right), \tag{10}$$

where $\varepsilon = 0.1$ is an angle that allows for a smooth transition of eq. (10) around $\theta_{\max}$. As an example, we initialize the pulse using $\theta_{\max} = 59°$, $\ell = 2\lambda$, $R_0 = 16\lambda$, and advance the electromagnetic field described by eqs. (8) and (10) within a quadratic box Ω_B with side lengths $2(R_0 + \ell)$ using the `field_loop_callback` in π-PIC. Then, a separate pulse initialization is done using the periodic mapping implementation (referred to as *periodic* in fig. 3) within a smaller domain Ω_b with side lengths 4λ. Both configurations have

8

a spatial resolution of 16 cells per wavelength and are evolved over a single time step R_0/c, yielding the initial and final electromagnetic field states as shown in fig. 3(a)–(d). The relative root-mean-square error for the electromagnetic energy density computed within the focal region, was found to be 1.43×10^{-4}, demonstrating the accuracy of the periodic mapping implementation. To assess the efficiency of periodic mapping, we benchmark the runtime using 8 Intel(R) Core(TM) i7-10700K CPUs for initializing the field and performing a single time step R_0/c as a function of R_0, while maintaining the same spatial resolution. This time, the box Ω_B is set to have dimensions $L_x = R_0 + \ell/2 + 2\lambda$ and $L_y = 2R_0 \sin(\varepsilon + \theta_{\max})$ so as to precisely enclose Ω_b and the pulse profile u. The resulting benchmark, presented in fig. 3(e), demonstrates a significant speed-up for the periodic mapping algorithm across all values of R_0.

5 Solvers

In π-PIC, the solver class is an object containing all code relevant to the PIC update. This functionality is, as mentioned in section 3, realized by two defining classes `pic_solver` and `field_solver`. Both classes has a number of mandatory and optional function with which different functionality can be implemented.

The `field_solver` has two mandatory methods: `fieldLoop` and `customFieldLoop`. The first implement a loop over the whole grid and the second a loop over a subset of coordinates. These methods are used by the Python interface and extensions to access data, it is therefore important that they are implemented by the developer since different solvers can feature different field grids.

The `pic_solver` class defines a single mandatory method, `advance`. Although its implementation is left to the developer, the recommended approach is to base it on the `advance_singleLoop` method in `ensemble.h`, since this routine handles additionally calls the extensions in a thread-safe and efficient manner. Due to the template-based structure of the code, and in order to avoid run-time compilation overhead, the developer is required to implement this function explicitly. The method `advance_singleLoop` will call the optional methods of `pic_solver`: `preStep()`, `preLoop()`, `startSubLoop()`, `processParticle()`, `endSubLoop()`, `postLoop()` and `postStep()` and, thereby, defines the execution order as below. Calls related to extensions, defined by the `handlerManager`, are highlighted in blue.

```
 1: preStep()
 2: for n in numberOfIterations:
 3:     apply_fieldHandlers()
 4:     preLoop()
 5:     for cell in CellInterface:
 6:         apply_actOnCellHandlers()
 7:         for particle type in cell:
 8:             startSubLoop()
 9:             apply_particleHandlers()
10:             for particle in particles of this type in cell:
11:                 processParticle()
12:             endSubLoop()
13:     postLoop()
14: postStep()
```

By organizing the PIC update into the optional methods of `pic_solver`, a wide range of PIC algorithms can be implemented while maintaining compatibility with extensions. As an example, we next present an electrostatic solver (section 5.1) that demonstrates how a solver can be constructed using this framework. The energy-conserving solver in π-PIC [15] can be complemented with an approximate momentum conservation scheme. This addition is described in section 5.2. We proceed by simulating laser wakefield acceleration (section 5.3) using two additional solvers of π-PIC: the Fourier-Boris (FB) solver – a spectral electromagnetic solver with Boris pusher – and the energy conserving (EC) solver [15]. As a benchmark, we compare the results with the same simulation performed by the PIC code Smilei [2] using the M4 solver [62].

5.1 Example: A electrostatic solver

To demonstrate the implementation of solvers a one-dimensional electrostatic solver was implemented in π-PIC. The solver advances the plasma state according to the electrostatic Vlasov equation and the

Ampere-Maxwell equation assuming zero magnetic field

$$\frac{\partial f}{\partial t} + v_x \frac{\partial f}{\partial x} + \frac{qE_x}{m}\frac{\partial f}{\partial v_x} = 0, \tag{11}$$

$$\frac{\partial E_x}{\partial t} + 4\pi j_x = 0. \tag{12}$$

The particle push corresponding to this system is $\partial_t v = \frac{qE_x}{m}$, which can be discretized using a forward finite difference scheme with time staggering

$$v_p^{j+1/2} = v_p^{j-1/2} + \frac{\Delta t q E_x^j(x_p^j)}{m}, \tag{13}$$

$$x_p^{j+1} = x_p^j + \Delta t v_p^{j+1/2} \tag{14}$$

where upper index denotes time step indices and lower particle index. The time staggering is realized through initializing v half a timestep backwards in time as $v_p^{-1/2} = v_p^0 - \frac{\Delta t q E_x^0(x_p^0)}{2m}$.

The electric field is advanced as

$$E_{x,i}^{j+1} = E_{x,i}^j - \Delta t 4\pi j_{x,i}^{j+1} \tag{15}$$

where upper indices denotes time indices and lower space indices. The current is interpolated to the grid from the particle position and momentum as

$$j_{x,i}^{j+1} = \sum_p^N wqS(x_p^{j+1} - x_i)v_p^{j+1/2} \tag{16}$$

where N is the number of particles, S is the shape function (Cloud-In-Cell), w is the macro-particle weight and the lower index denotes particle index. The electric field is interpolated back to the particle position similarly

$$E_x^j(x) = \sum_i^{N_g} S(x_i - x)E_{x,i}^j \tag{17}$$

where N_g are the number of adjacent grid nodes to x.

The relevant code for `pic_solver` and `field_solver` can be found in section B.1 and section B.2 respectively, however, in short this is how the methods in `pic_solver` was used to execute the algorithm: Apart from evolving the system according to eqs. (11) and (12), to accurately model the electrostatic

---

1: `preStep()` - Pull back particle velocities $\Delta t/2$ to implement staggered grid.
2: `preLoop()` - Advance E_x and set current to 0 everywhere.
3: `processParticle()` - Interpolate field to particle position, advance particle and deposit current.
4: `postStep()` - Advance particle velocities $\Delta t/2$ to remove staggering.

---

system, the discretization must also satisfy

$$\left.\begin{array}{l} \nabla \cdot \mathbf{E} = 4\pi\rho \\ \nabla \times \mathbf{E} = 0 \leftrightarrow \mathbf{E} = -\nabla\phi \end{array}\right\} \xrightarrow{\text{1D}} 4\pi\rho + \frac{\partial^2 \phi}{\partial \mathrm{x}^2} = 0.$$

This requires the system to be initialize in a state consistent with these equations. As the simulation progresses, this relation will be approximately maintained since the continuity equation (derivable from eq. (11) by integrating with respect to velocity) together with eq. (12) imposes

$$\frac{\partial}{\partial t}\left(\rho - \frac{1}{4\pi}\frac{\partial}{\partial x}E_x\right) = \frac{\partial}{\partial t}\left(\rho + \frac{1}{4\pi}\frac{\partial^2 \phi}{\partial x^2}\right) = 0. \tag{18}$$

However, this restricts the plasma systems which can be realistically simulated using periodic boundary conditions to systems with zero spatial average charge and current. Nevertheless, with this simple set of equations is possible to simulate quasi-electrostatic phenomenons such as plasma oscillations and the early stages of charge-current neutral two-stream instability as demonstrated in fig. 4.
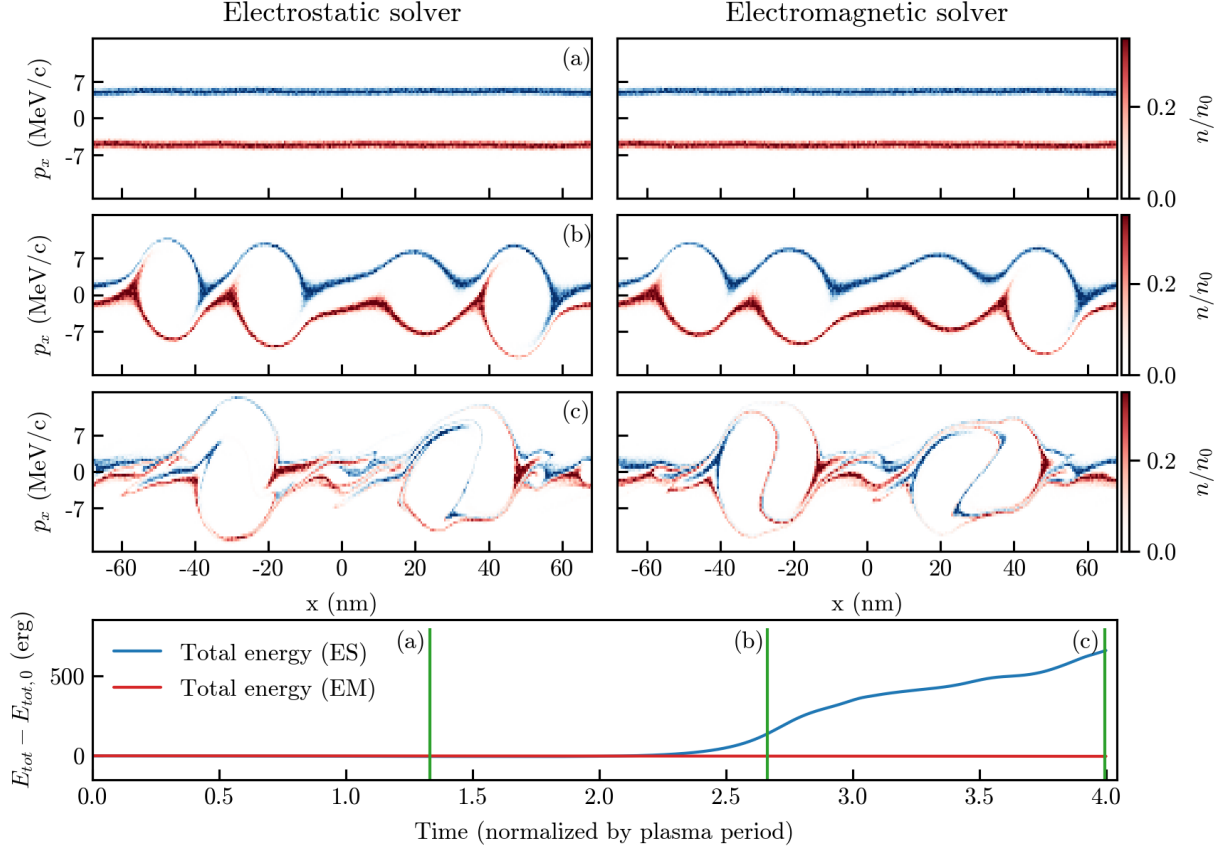
Figure 4: A two-stream instability by initializing opposite and equal currents flowing in a constant background field. The instability was simulated using two solvers: (left) electrostatic solver and (right) a electromagnetic solver (spectral field solver with Boris particle pusher). The density perturbation in phase space, n, is normalized to the initial particle density n_0. The electrostatic solver resolves the excitation of the two stream instability, but as the instability grows - the electrostatic simulation starts to gain total energy and eventually becomes invalid.

5.2 Energy-conservative and momentum semi-conservative solver

In this section, we describe an explicit, relativistic, second-order PIC solver that exactly preserves energy and is improved in relation to momentum conservation. The idea is based on splitting the deviation from exact preservation of these physically conserved quantities into three fundamental contributions and eliminating two of them. In doing this analysis, we indicate the path towards eliminating the last contribution as well. That is why this solver represents an essential step towards a possible way for simultaneous conservation of both energy and momentum.

Our approach is based on a modification of the PIC method proposed and used to achieve energy conservation in Ref. [15]. This modification exploits a particle-wise splitting of the Maxwell-Vlasov set of equations such that the current in Maxwell's equations and the electric component of the Lorentz force are accounted for within a single subsystem for each particle. This means that the state of each particle is coupled with the state of electromagnetic field in the nearby nodes, resulting in the evolution equation that can be solved with enforced energy conservation. Here, we extend this approach to also enforce the exact conservation of momentum related to the magnetic component of the Lorentz force.

We start by considering the energy and momentum exchange between the electromagnetic field and a single charge. For this auxiliary analysis, we assume that the charge is distributed within a rigid body, the center of which is at $\mathbf{r}_b$. By considering the effect of all the terms in the Maxwell-Vlasov set of equations, we separate the part that is responsible for the energy and momentum exchange (CGS units

are used):

$$\frac{\partial}{\partial t}\mathbf{E}\left(\mathbf{r}\right) = -4\pi\mathbf{J}\left(\mathbf{r}\right), \tag{19}$$

$$\mathbf{J}\left(\mathbf{r}\right) = \rho\left(\mathbf{r}-\mathbf{r}_b\right)\frac{c}{\gamma}\mathbf{p}_b, \tag{20}$$

$$\frac{\partial}{\partial t}\mathbf{p}_b = \frac{1}{m_b c}\int_{V_b}\rho(\mathbf{r}-\mathbf{r}_b)\left(\mathbf{E}\left(\mathbf{r}\right)+\frac{c}{\gamma}\mathbf{p}_b\times\mathbf{B}\left(\mathbf{r}\right)\right)dr, \tag{21}$$

where $\mathbf{B}$, $\mathbf{E}$ are magnetic and electric field vectors; $\mathbf{J}$ is the charge current; c is the speed of light, m_b, $\rho(\mathbf{r}-\mathbf{r}_b)$, $\mathbf{p}_b$ and $\gamma = \sqrt{1+p_b^2}$ are the mass, charge density, momentum (given in units of $m_b c$) and gamma factor of the rigid body in consideration, while V_b denotes the part of the space occupied by the body. The first equation describes the account of current in Maxwell's equations, the second is the definition of current and the third describes cumulative effect of the Lorentz force on the change of momentum. To see the origin of energy conservation in this system, we consider time derivative of the total energy W being a sum of electromagnetic energy and the kinetic energy of the body in question:

$$\frac{\partial}{\partial t}W = \frac{\partial}{\partial t}\left(\int\frac{E^2(\mathbf{r})+B^2(\mathbf{r})}{8\pi}dr + m_b c^2\gamma\right) \overset{!}{=} 0. \tag{22}$$

Since the magnetic field is not altered by any of eqs. (19) to (21) and electric field is modified only within V_b, we can write

$$0 \overset{!}{=} \frac{\partial}{\partial t}W = \int_{V_b}\frac{1}{4\pi}\mathbf{E}\cdot\frac{\partial\mathbf{E}}{\partial t}dr + \frac{m_b c^2}{\gamma}\mathbf{p}_b\cdot\frac{\partial\mathbf{p}_b}{\partial t}. \tag{23}$$

Substituting the electric component of the Lorentz force to the second term (the magnetic component does no work) and using eqs. (19) and (20) to express $\partial\mathbf{E}/\partial t$ in the first term, we obtain:

$$\frac{\partial}{\partial t}W = -\int_{V_b}\frac{c}{\gamma}\mathbf{E}\cdot\mathbf{p}_b\rho(\mathbf{r}-\mathbf{r}_b)dr + \frac{c}{\gamma}\mathbf{p}_b\cdot\left(\int_{V_b}\mathbf{E}\rho\left(\mathbf{r}-\mathbf{r}_b\right)dr\right) = 0. \tag{24}$$

This indicates that the system given by eqs. (19) to (21) describes the changed of field and particle states in accordance with energy conservation, while the electric component of Lorentz force is the one that is responsible for this. To see the role of magnetic component of the Lorenz force, we can consider it separately:

$$\frac{\partial}{\partial t}\mathbf{p}_b^{(B)} = \frac{1}{m_b c}\int_{V_b}\rho(\mathbf{r}-\mathbf{r}_b)\frac{c}{\gamma}\mathbf{p}_b\times\mathbf{B}dr. \tag{25}$$

Using eqs. (19) and (20), we obtain (note that $\mathbf{B}$ is not changed by eqs. (19) to (21)):

$$\frac{\partial}{\partial t}\mathbf{p}_b^{(B)} = \int_{V_b}\mathbf{J}\times\mathbf{B}dr = -\frac{\partial}{\partial t}\int\frac{1}{4\pi}\mathbf{E}\times\mathbf{B}dr. \tag{26}$$

On the right hand side, to within a factor of c, we have time derivative of the Poynting vector $(c/4\pi)\,\mathbf{E}\times\mathbf{B}$, which describes energy flux of electromagnetic field. Since a photon carrying energy $\hbar\omega$ carries momentum $\hbar\mathbf{k} = (\hbar\omega/c)\mathbf{k}/k$, we can interpret this as an equation that describes the transfer of momentum carried by electromagnetic waves to $\mathbf{p}_b$ and vice versa. The remaining part of momentum conservation concerns the exchange of momentum between the body and electrostatic field.

In such a way we can observe three essential channels for the deviation from the exact conservation of energy and momentum. The first one concerns energy conservation and can be eliminated by coupling the update of particle momentum due to the electric component of the Lorentz force with the update of electric field due to current induced by this particle (this has been done in Ref. [15]). The second channel concerns momentum exchange between photons and the particle in question (eq. (26)). Analogously, this channel can be eliminated by coupling the update of electric field with the update of particle momentum, but now due to both electric and magnetic components of the Lorentz force. Finally, the last channel concerns momentum exchange between the particle and electrostatic part of the field. Eliminating this last channel requires adding to the subsystem the account for the charge deposition that must be coupled with current in a way that exactly complies with the charge continuity equation. Unfortunately, exact local agreement with the charge continuity equation is inconsistent with the Fourier solver (approximate agreement can be enhanced by the use of higher-order particle shapes). Nevertheless, it is interesting to consider the use of Esirkepov charge conservation scheme [63] in combination with the consecrative

update of electromagnetic field within the framework of finite element exterior calculus [64,65]. Leaving this consideration for future work, we here describe the elimination of the second channel that can be seen as an essential step for this approach.

To eliminate the first and the second channels of deviations from the energy-momentum conservations we need to find exact solution of the following system:

$$\frac{\partial \mathbf{p}}{\partial t} = \frac{q}{mc}\mathbf{E} + \frac{q}{mc\gamma}\mathbf{p} \times \mathbf{B}, \tag{27}$$

$$\frac{\partial \mathbf{E}}{\partial t} = -4\pi \mathbf{J}, \tag{28}$$

where q and m are the charge and mass of the particle, whereas $\mathbf{J}$, $\mathbf{E}$ and $\mathbf{B}$ are the weighted current, electric and magnetic field, respectively. The weighting is defined by weight coefficients c_i (given the use of Fourier method we here assume collocated grids for all quantities and use subscript to indicate grid node):

$$\mathbf{E} = \sum c_i \mathbf{E}_i, \tag{29}$$

$$\mathbf{B} = \sum c_i \mathbf{B}_i, \tag{30}$$

$$\mathbf{J} = \sum c_i \frac{qc}{V_g} \frac{\mathbf{p}}{\gamma}, \tag{31}$$

where V_g is the volume of a grid cell. Taking time derivative of eq. (27) and substituting $\mathbf{E}/\partial t$ from eq. (28), we obtain:

$$\frac{\partial^2}{\partial t^2}\mathbf{p} = -\frac{\eta}{\gamma}\mathbf{p} + \frac{q}{mc\gamma}\left(\frac{\partial}{\partial t}\mathbf{p}\right) \times \mathbf{B}, \tag{32}$$

$$\eta = \frac{4\pi q^2 \sum c_i^2}{mV_g}. \tag{33}$$

We use the approach of effective mass, considering γ fixed under this update and using correction later (see [15]). Introducing rescaled time, electric and magnetic field:

$$\tau = \sqrt{\frac{\eta}{\gamma}}t, \tag{34}$$

$$\mathbf{b} = \frac{q}{mc\sqrt{\eta\gamma}}\mathbf{B}, \tag{35}$$

$$\mathbf{e} = \sqrt{\frac{\gamma}{\eta}}\frac{q}{mc}\mathbf{E} \tag{36}$$

we obtain

$$\ddot{\mathbf{p}} = -\mathbf{p} + \dot{\mathbf{p}} \times \mathbf{b}, \tag{37}$$

$$\dot{\mathbf{p}} = \mathbf{e} + \mathbf{p} \times \mathbf{b}, \tag{38}$$

where we use dot to denote time derivative with respect to rescaled time τ. We now need to solve eq. (37) with initial conditions given by particle's initial $\mathbf{p}$ and $\dot{\mathbf{p}}$ defined via eq. (38) for the initial electric field. The value of $\dot{\mathbf{p}}$ after one time step defines the updated value of the electric field.

To solve eq. (37), we introduce an orthogonal basis with one axis being parallel to $\mathbf{b}$. Let us denote the component of $\mathbf{b}$ along this axis by p_3 and the two other components by p_1 and p_2. Then for p_3 we have harmonic oscillator equation:

$$\ddot{p}_3 + p_3 = 0, \tag{39}$$

the exact solution of which can be expressed using sine and cosine function computation for the given time step. For the other two components we obtain:

$$\ddot{p}_1 = -p_1 + \dot{p}_2 b, \tag{40}$$

$$\ddot{p}_2 = -p_2 - \dot{p}_1 b. \tag{41}$$

Introducing four-component vector

$$s = (\dot{p}_1, \dot{p}_2, p_1, p_2)^T, \tag{42}$$

13

we can transform these set of equation into matrix form

$$\dot{s} = As, \; A = \begin{pmatrix} 0 & b & -1 & 0 \\ -b & 0 & 0 & -1 \\ 1 & 0 & 0 & 0 \\ 0 & 1 & 0 & 0 \end{pmatrix}. \tag{43}$$

Following standard procedure we transform this matrix equation into the one with diagonal matrix by transforming the basis. Under such transformation the diagonal elements have the form:

$$w_{1,2,3,4} = \pm \frac{i}{\sqrt{2}} \left(b^2 + 2 \pm b \left(b^2 + 4 \right)^{1/2} \right)^{1/2}. \tag{44}$$

The exact solution can then be expressed using two sine and cosine function computations. This procedure is implemented in π-PIC for the second-order solver that is available under the name `emc2`. The implementation follows the outline patterns [45].

5.3 Benchmark: Laser wake-field acceleration

PIC codes are widely used for the simulation of laser wakefield acceleration (LWFA). Since its proposal [66], the acceleration technique has attracted much attention because it can sustain accelerating gradients that far exceed those produced by conventional accelerators [67], thereby enabling compact sources of relativistic particles.

In this section, we will benchmark simulations of LWFA using the energy-conserving solver [15] and the Fourier-Boris (FB) solver of π-PIC, comparing it against the well-established PIC-code Smilei [2]. In particular, we will focus on performance at low-resolution. The FB solver is a standard spectral solver with a Boris particle-pusher. For simulations with Smilei we use the M4 maxwell solver [62] since it exhibits reduced numerical dispersion, which slows down the propagation of electro-magnetic waves, compared to the standard FDTD solver. In contrast the energy-conserving and FB solver in π-PIC uses as spectral solver, which inherently avoids this problem.

We begin by simulating the one-dimensional wakefield excitation that occurs when a laser interacts with a plasma density upramp.. We employ a laser with wavelength $\lambda = 1 \, \mu m$ and a Gaussian time-envelope spanning 30 laser cycles at full width half maximum (FWHM). The laser envelope has a peak amplitude $a_0 = e|E|/(m_e c \omega) = 4$, where e denotes the electron charge, E the electric field amplitude, m_e the electron mass, c the speed of light and ω the laser frequency. The plasma density ramps from 0 to $4 \cdot 10^{18} \, cm^{-3}$ in $2^{10} \lambda = 1024 \, \mu m$. The simulations have a space step $\Delta x = \lambda/16$, time step $\Delta t = \lambda/(64c)$ and 8 particles per cell.

The 1D simulations, shown in fig. 5 shows near excellent agreement except for a minor difference in the build up of the longitudinal electric field, see fig. 5.c. However, the EC and FB solver shows absolute agreement.
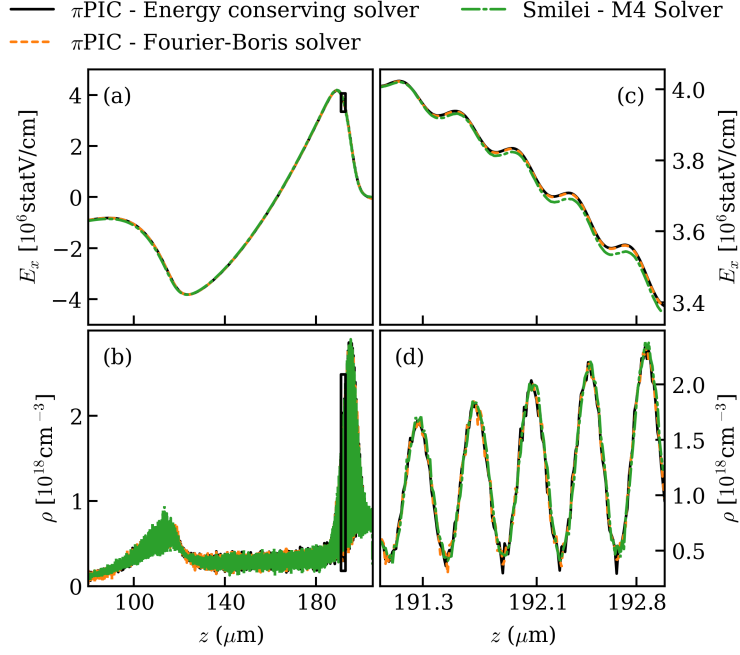
Figure 5: Longitudinal electric field (a, c) and plasma density (b, d) for 1D LWFA simulations using π-PIC with EC and FB solver as well as Smilei with M4 solver. The black rectangles in (a) and (b) indicate the enlarged area shown in (c) and (d) respectively.

Having shown satisfactory agreement in 1D we move on to full 3D simulations of LWFA, where additionally injection and subsequent acceleration of particles is simulated. This is achieved via density downramp injection, using a plasma profile that decreases to one-third of the peak density ($n_e = 4 \cdot 10^{18}, \mathrm{cm}^{-3}$) at the end of the upramp, see fig. 6(d). The simulation parameters for the laser are identical to the 1D case, with the addition of laser focusing, characterized by a focus at the position of the downramp with a spot size of 40λ. While the results in fig. 6 are qualitatively similar, the on-axis accelerating fields vary in amplitude and bubble-length between π-PIC and Smilei, despite the wave fronts being identical. Moreover, there is a noticeable difference in the amount of injected charge and the resulting phase-space distribution of the accelerated beam.

The observed differences in particle injection suggest that the discrepancy between the solvers arises from their distinct shape functions. Smilei employs a 3-point stencil, whereas π-PIC uses a CIC shape function corresponding to a 1-point stencil. In addition, Smilei enforces exact charge conservation through Esirkepov's deposition scheme [27]. In contrast, the solvers in π-PIC do not implement a similar deposition scheme; however, the FBs solver applies a Poisson-based charge correction. The agreement in plasma response between the EC and FB solvers indicates that charge non-conservation does not account for the differences observed between the π-PIC and Smilei solvers, pointing instead to the shape function as the most probable source of the discrepancy. Since the FB and energy-conserving solvers are once again in complete agreement, we have excluded FB from the subsequent simulations.
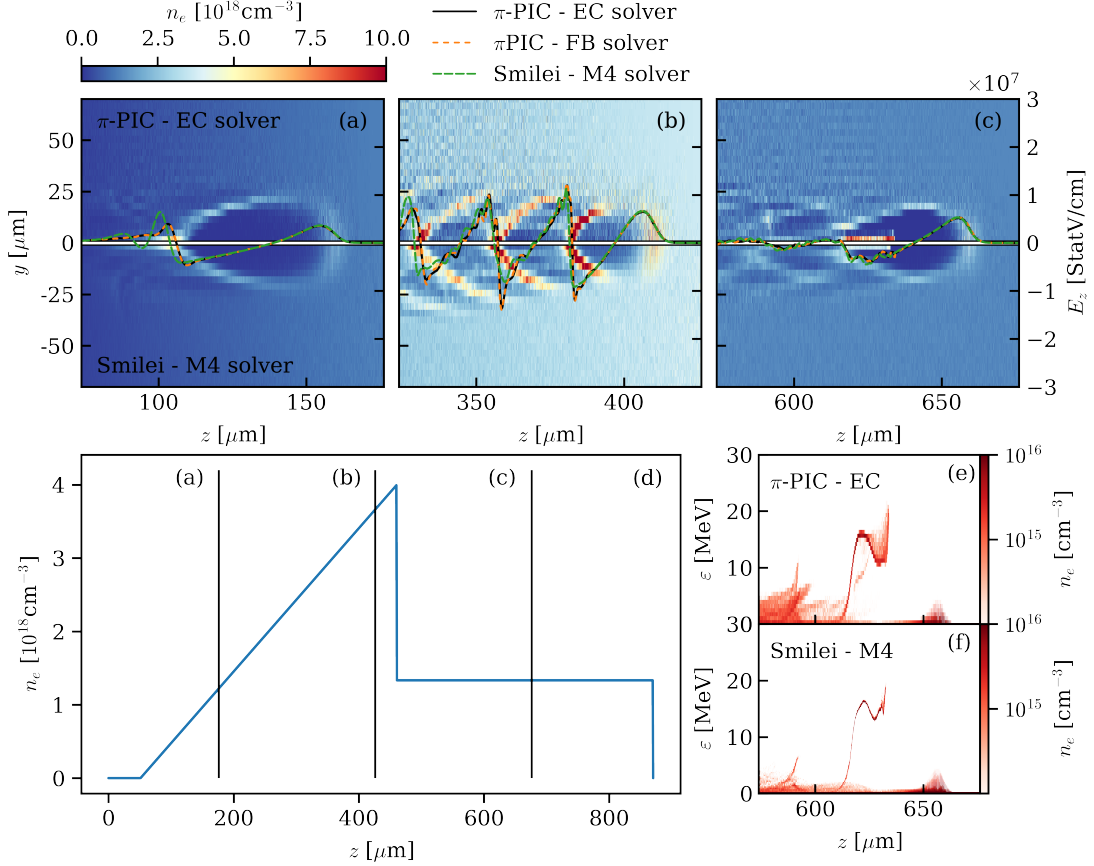
Figure 6: Panel (a-c) shows the on-axis density at three different positions in the plasma marked in panel (d). The upper half of (a-c) shows the π-PIC simulation and the lower the Smilei simulation, additionally the on-axis electric field is shown in for π-PIC using the EC solver (full black) and FB solver (dashed orange) as well as the M4 solver of Smilei (green dashed). Panel (e-f) shows the phase-space at the longitudinal position corresponding to subplot (c).

To look further into these differences, we perform several simulations with different spatial and temporal resolutions, as shown in fig. 7. The timestep was $\Delta t = \Delta x/(c4)$ and $\Delta y = \Delta x = 4\lambda$. At high resolution ($\Delta x = \lambda/32$), Smilei and π-PIC show strong agreement at the front of the wake, but a qualitative difference emerges at the rear end of the wake. Additionally, Smilei converges to a solution faster with resolution, as the electric field for $\Delta x = \lambda/32$ and $\Delta x = \lambda/16$ is practically identical – which is not the case for π-PIC.

For lower resolution there is a decrease in impact of the laser for both codes, shown at the front of the wake. This is to be expected, since the ponderomotive force which drives the wake, is an averaged force and by under-sampling the oscillations of the field the particles experience a lower effective push. For π-PIC there is also an effective decrease of plasma wavelength for lower resolutions. Smilei, on the other hand, shows a decrease in propagation speed of the wake which becomes progressively worse with resolution. At a resolution of $n_x/\lambda = 4$ (red line) the head of the wake is almost out of window.

In conclusion, we find that π-PIC retains a higher degree of accuracy at low resolution but the convergence of the code with higher resolution is weak compared to Smilei.

Figure 7: Shows the longitudinal electric field at the plasma upramp corresponding to position (a) in fig. 6 for simulations of π-PIC (upper) and Smilei (lower) for different resolutions.

6   Conclusion

PIC methods provide powerful tools for studying plasmas across a wide range of environments and scales. The expansion of computing power makes previously unfeasible simulations achievable. Despite significant progress and ongoing research, challenges remain regarding numerical stability and conservation properties. To accommodate further research, we have developed a flexible PIC framework, which enables users to modify and extend the PIC scheme. Its modular structure supports parallel development on multiple levels, such as solver and extension implementation, with the aim of making it a valuable resource for the broader plasma community.

17

References

[1] H. Burau, R. Widera, W. Hönig, G. Juckeland, A. Debus, T. Kluge, U. Schramm, T. E. Cowan, R. Sauerbrey, and M. Bussmann, "PIConGPU: A fully relativistic particle-in-cell code for a GPU cluster," *IEEE Transactions on Plasma Science*, vol. 38, no. 10, pp. 2831–2839, 2010.

[2] J. Derouillat, A. Beck, F. Pérez, T. Vinci, M. Chiaramello, A. Grassi, M. Flé, G. Bouchard, I. Plotnikov, N. Aunai, J. Dargent, C. Riconda, and M. Grech, "Smilei : A collaborative, open-source, multipurpose particle-in-cell code for plasma simulation," *Comput. Phys. Commun.*, vol. 222, pp. 351–373, 2018.

[3] R. A. Fonseca, L. O. Silva, F. S. Tsung, V. K. Decyk, W. Lu, C. Ren, W. B. Mori, S. Deng, S. Lee, T. Katsouleas, and J. C. Adam, "OSIRIS: A three-dimensional, fully relativistic particle in cell code for modeling plasma based accelerators," in *Computational Science — ICCS 2002* (P. M. A. Sloot, A. G. Hoekstra, C. J. K. Tan, and J. J. Dongarra, eds.), pp. 342–351, Springer, 2002.

[4] S. Bastrakov, R. Donchenko, A. Gonoskov, E. Efimenko, A. Malyshev, I. Meyerov, and I. Surmin, "Particle-in-cell plasma simulation on heterogeneous cluster systems," *Journal of Computational Science*, vol. 3, no. 6, pp. 474–479, 2012.

[5] J. L. Vay, A. Almgren, J. Bell, L. Ge, D. P. Grote, M. Hogan, O. Kononenko, R. Lehe, A. Myers, C. Ng, J. Park, R. Ryne, O. Shapoval, M. Thévenet, and W. Zhang, "Warp-x: A new exascale computing platform for beam–plasma simulations," *Nuclear Instruments and Methods in Physics Research Section A: Accelerators, Spectrometers, Detectors and Associated Equipment*, vol. 909, pp. 476–479, 2018.

[6] R. Lehe, M. Kirchen, I. A. Andriyash, B. B. Godfrey, and J.-L. Vay, "A spectral, quasi-cylindrical and dispersion-free particle-in-cell algorithm," *Comput. Phys. Commun.*, vol. 203, pp. 66–82, 2016.

[7] OpenFOAM Foundation, "OpenFOAM: The Open Source CFD Toolbox." https://www.openfoam.com/. Accessed: 2025-08-20.

[8] Atomic Simulation Environment (ASE), "ASE: Atomic Simulation Environment." https://wiki.fysik.dtu.dk/ase/. Accessed: 2025-08-20.

[9] LAMMPS Development Team, "LAMMPS Molecular Dynamics Simulator." https://www.lammps.org/. Accessed: 2025-08-20.

[10] BLAS Working Group, "Basic Linear Algebra Subprograms (BLAS)." http://www.netlib.org/blas/. Accessed: 2025-08-20.

[11] LAPACK Project, "LAPACK: Linear Algebra PACKage." http://www.netlib.org/lapack/. Accessed: 2025-08-20.

[12] Frigo, Matteo and Johnson, Steven G., "FFTW: Fastest Fourier Transform in the West." http://www.fftw.org/. Accessed: 2025-08-20.

[13] COIN-OR Foundation, "COIN-OR: Computational Infrastructure for Operations Research." https://www.coin-or.org/. Accessed: 2025-08-20.

[14] Pedregosa, Fabian and Varoquaux, Gaël and Gramfort, Alexandre and Michel, Vincent and others, "Scikit-learn: Machine Learning in Python." https://scikit-learn.org/. Accessed: 2025-08-20.

[15] A. Gonoskov, "Explicit energy-conserving modification of relativistic pic method," *J. Comput. Phys.*, vol. 502, p. 112820, Apr. 2024.

[16] K. Yee, "Numerical solution of initial boundary value problems involving maxwell's equations in isotropic media," *IEEE Transactions on Antennas and Propagation*, vol. 14, no. 3, pp. 302–307, 1996.

[17] A. Pukhov, "Three-dimensional electromagnetic relativistic particle-in-cell code VLPL (virtual laser plasma lab)," *Journal of Plasma Physics*, vol. 61, no. 3, pp. 425–433, 1999.

[18] M. Kärkkäinen, E. Gjonaj, T. Lau, and T. Weiland, "Low-dispersion wake field calculation tools," *Proc. International Computational Accelerator Physics Conference*, 01 2006.

[19] J. Cole, "A high-accuracy realization of the yee algorithm using non-standard finite differences," *IEEE Transactions on Microwave Theory and Techniques*, vol. 45, no. 6, pp. 991–996, 1997.

[20] R. Lehe, A. Lifschitz, C. Thaury, V. Malka, and X. Davoine, "Numerical growth of emittance in simulations of laser-wakefield acceleration," *Physical Review Special Topics - Accelerators and Beams*, vol. 16, no. 2, p. 021301, 2013.

[21] B. M. Cowan, D. L. Bruhwiler, J. R. Cary, E. Cormier-Michel, and C. G. R. Geddes, "Generalized algorithm for control of numerical dispersion in explicit time-domain electromagnetic simulations," *Physical Review Special Topics - Accelerators and Beams*, vol. 16, no. 4, p. 041303, 2013.

[22] C. K. Birdsall and A. B. Langdon, *Plasma Physics via Computer Simulation*. CRC Press, 2018.

[23] J.-L. Vay, I. Haber, and B. B. Godfrey, "A domain decomposition method for pseudo-spectral electromagnetic simulations of plasmas," *J. Comput. Phys.*, vol. 243, pp. 260–268, 2013.

[24] B. Marder, "A method for incorporating gauss' law into electromagnetic PIC codes," *J. Comput. Phys.*, vol. 68, no. 1, pp. 48–55, 1987.

[25] C. D. Munz, P. Omnes, R. Schneider, E. Sonnendrücker, and U. Voß, "Divergence correction techniques for maxwell solvers based on a hyperbolic model," *J. Comput. Phys.*, vol. 161, no. 2, pp. 484–511, 2000.

[26] J. Villasenor and O. Buneman, "Rigorous charge conservation for local electromagnetic field solvers," *Comput. Phys. Commun.*, vol. 69, no. 2, pp. 306–316, 1992.

[27] T. Z. Esirkepov, "Exact charge conservation scheme for particle-in-cell simulation with an arbitrary form-factor," *Comput. Phys. Commun.*, vol. 135, no. 2, pp. 144–153, 2001.

[28] T. Umeda, Y. Omura, T. Tominaga, and H. Matsumoto, "A new charge conservation method in electromagnetic particle-in-cell simulations," *Comput. Phys. Commun.*, vol. 156, no. 1, pp. 73–85, 2003.

[29] X. Kong, M. C. Huang, C. Ren, and V. K. Decyk, "Particle-in-cell simulations with charge-conserving current deposition on graphic processing units," *J. Comput. Phys.*, vol. 230, no. 4, pp. 1676–1685, 2011.

[30] K. Steiniger, R. Widera, S. Bastrakov, M. Bussmann, S. Chandrasekaran, B. Hernandez, K. Holsapple, A. Huebl, G. Juckeland, J. Kelling, M. Leinhauser, R. Pausch, D. Rogers, U. Schramm, J. Young, and A. Debus, "EZ: An efficient, charge conserving current deposition algorithm for electromagnetic particle-in-cell simulations," *Comput. Phys. Commun.*, vol. 291, p. 108849, 2023.

[31] A. Pukhov, "Particle-in-cell codes for plasma-based particle acceleration," *CERN Yellow Reports*, vol. 1, pp. 181–181, 2016.

[32] A. T. Powis and I. D. Kaganovich, "Accuracy of the explicit energy-conserving particle-in-cell method for under-resolved simulations of capacitively coupled plasma discharges," *Phys. Plasmas*, vol. 31, no. 2, p. 023901, 2024.

[33] A. B. Langdon, "Effects of the spatial grid in simulation plasmas," *J. Comput. Phys.*, vol. 6, no. 2, pp. 247–267, 1970.

[34] R. W. Hockney and J. W. Eastwood, *Computer Simulation Using Particles*, ch. 5-5, p. 149. CRC Press, 2021.

[35] L. F. Ricketson and J. Hu, "An explicit, energy-conserving particle-in-cell scheme," *J. Comput. Phys.*, vol. 537, p. 114098, Sept. 2025.

[36] J. Xiao, H. Qin, and J. Liu, "Structure-preserving geometric particle-in-cell methods for vlasov-maxwell systems," *Plasma Science and Technology*, vol. 20, no. 11, p. 110501, 2018.

[37] J. Squire, H. Qin, and W. M. Tang, "Geometric integration of the vlasov-maxwell system with a variational particle-in-cell scheme," *Phys. Plasmas*, vol. 19, no. 8, p. 084501, 2012.

[38] M. Kraus, K. Kormann, P. J. Morrison, and E. Sonnendrücker, "GEMPIC: geometric electromagnetic particle-in-cell methods," *Journal of Plasma Physics*, vol. 83, no. 4, p. 905830401, 2017.

[39] K. Kormann and E. Sonnendrücker, "Energy-conserving time propagation for a structure-preserving particle-in-cell vlasov–maxwell solver," *J. Comput. Phys.*, vol. 425, p. 109890, 2021.

[40] A. Gonoskov, S. Bastrakov, E. Efimenko, A. Ilderton, M. Marklund, I. Meyerov, A. Muraviev, A. Sergeev, I. Surmin, and E. Wallin, "Extended particle-in-cell schemes for physics in ultrastrong laser fields: Review and developments," *Physical review E*, vol. 92, no. 2, p. 023305, 2015.

[41] V. Volokitin, J. Magnusson, A. Bashinov, E. Efimenko, A. Muraviev, and I. Meyerov, "Optimized event generator for strong-field qed simulations within the hi-chi framework," *Journal of Computational Science*, vol. 74, p. 102170, 2023.

[42] A. Gonoskov, "Agnostic conservative down-sampling for optimizing statistical representations and PIC simulations," *Comput. Phys. Commun.*, vol. 271, p. 108200, Feb. 2022.

[43] A. Muraviev, A. Bashinov, E. Efimenko, V. Volokitin, I. Meyerov, and A. Gonoskov, "Strategies for particle resampling in PIC simulations," *Comput. Phys. Commun.*, vol. 262, p. 107826, May 2021.

[44] W. Jakob, "pybind11: Seamless interoperability between C++ and Python." https://pybind11.readthedocs.io/en/stable/. Accessed: 2025-09-30.

[45] hi chi, "π-pic: A python-controlled interactive particle-in-cell code." https://github.com/hi-chi/pipic/tree/pipic_tutorial, 2023. [Code].

[46] J.-P. Berenger, "A perfectly matched layer for the absorption of electromagnetic waves," *J. Comput. Phys.*, vol. 114, no. 2, pp. 185–200, 1994.

[47] T. Tajima and Y. C. Lee, "Absorbing boundary condition and budden turning point technique for electromagnetic plasma simulations," *J. Comput. Phys.*, vol. 42, no. 2, pp. 406–412, 1981.

[48] G. A. Mourou, T. Tajima, and S. V. Bulanov, "Optics in the relativistic regime," *Reviews of Modern Physics*, vol. 78, p. 309–371, Apr. 2006.

[49] M. Marklund and P. K. Shukla, "Nonlinear collective effects in photon-photon and photon-plasma interactions," *Reviews of Modern Physics*, vol. 78, p. 591–640, May 2006.

[50] A. Di Piazza, C. Müller, K. Z. Hatsagortsyan, and C. H. Keitel, "Extremely high-intensity laser interactions with fundamental quantum systems," *Reviews of Modern Physics*, vol. 84, p. 1177–1228, Aug. 2012.

[51] F. Krausz and M. Ivanov, "Attosecond physics," *Reviews of Modern Physics*, vol. 81, p. 163–234, Feb. 2009.

[52] L. W. Davis, "Theory of electromagnetic beams," *Physical Review A*, vol. 19, p. 1177–1179, Mar. 1979.

[53] M. Couture and P.-A. Belanger, "From gaussian beam to complex-source-point spherical wave," *Physical Review A*, vol. 24, p. 355–359, July 1981.

[54] A. M. Fedotov, K. Y. Korolev, and M. V. Legkov, "Exact analytical expression for the electromagnetic field in a focused laser beam or pulse," in *ICONO 2007: Physics of Intense and Superintense Laser Fields; Attosecond Pulses; Quantum and Atomic Optics; and Engineering of Quantum Information* (M. V. Fedorov, W. Sandner, E. Giacobino, S. Kilin, S. Kulik, A. Sergienko, A. Bandrauk, and A. M. Sergeev, eds.), vol. 6726, p. 672613, SPIE, June 2007.

[55] S. M. Sepke and D. P. Umstadter, "Analytical solutions for the electromagnetic fields of tightly focused laser beams of arbitrary pulse length," *Optics Letters*, vol. 31, p. 2589, Aug. 2006.

[56] Y. Salamin, "Fields of a gaussian beam beyond the paraxial approximation," *Applied Physics B*, vol. 86, p. 319–326, Sept. 2006.

[57] K. I. Popov, V. Y. Bychenkov, W. Rozmus, and R. D. Sydora, "Electron vacuum acceleration by a tightly focused laser pulse," *Phys. Plasmas*, vol. 15, Jan. 2008.

[58] D. E. Cardenas, T. M. Ostermayr, L. Di Lucchio, L. Hofmann, M. F. Kling, P. Gibbon, J. Schreiber, and L. Veisz, "Sub-cycle dynamics in relativistic nanoplasma acceleration," *Scientific Reports*, vol. 9, May 2019.

[59] A. A. Gonoskov, A. V. Korzhimanov, A. V. Kim, M. Marklund, and A. M. Sergeev, "Ultrarelativistic nanoplasmonics as a route towards extreme-intensity attosecond pulses," *Physical Review E*, vol. 84, Oct. 2011.

[60] C. Harvey, M. Marklund, and A. R. Holkundkar, "Focusing effects in laser-electron thomson scattering," *Physical Review Accelerators and Beams*, vol. 19, Sept. 2016.

[61] E. Panova, V. Volokitin, E. Efimenko, J. Ferri, T. Blackburn, M. Marklund, A. Muschet, A. De Andres Gonzalez, P. Fischer, L. Veisz, *et al.*, "Optimized computation of tight focusing of short pulses using mapping to periodic space," *Applied Sciences*, vol. 11, no. 3, p. 956, 2021.

[62] Y. Lu, P. Kilian, F. Guo, H. Li, and E. Liang, "Time-step dependent force interpolation scheme for suppressing numerical cherenkov instability in relativistic particle-in-cell simulations," *J. Comput. Phys.*, vol. 413, p. 109388, 2020.

[63] T. Esirkepov, "Exact charge conservation scheme for particle-in-cell simulation with an arbitrary form-factor," *Comput. Phys. Commun.*, vol. 135, pp. 144–153, Apr. 2001.

[64] D. N. Arnold, R. S. Falk, and R. Winther, "Finite element exterior calculus, homological techniques, and applications," *Acta Numerica*, vol. 15, p. 1–155, May 2006.

[65] M. Kraus, K. Kormann, P. J. Morrison, and E. Sonnendrücker, "Gempic: geometric electromagnetic particle-in-cell methods," *Journal of Plasma Physics*, vol. 83, July 2017.

[66] T. Tajima and J. M. Dawson, "Laser electron accelerator," *Physical Review Letters*, vol. 43, no. 4, pp. 267–270, 1979.

[67] E. Esarey, C. B. Schroeder, and W. P. Leemans, "Physics of laser-driven plasma-based electron accelerators," *Reviews of Modern Physics*, vol. 81, no. 3, pp. 1229–1285, 2009.

A Example script

```python
''' Description: this file demonstrates the use of the absorbing boundaries
    extension
to simulate plasma oscillations in a 1D plasma with open boundaries. The absorbing
boundaries extension removes particles leaving the simulation box and adds new
particles according to a specified density profile, simulating an open plasma system
    .
The script uses the absorbing boundary extension installable with pipic.
For more details on installtion and usage of the extension, please refer to:
https://github.com/hi-chi/pipic/blob/main/docs/guides/EXTENSION_DEVELOPMENT.md and
https://github.com/hi-chi/pipic/blob/main/docs/EXTENSIONS.md'''
import pipic
from pipic import consts, types
import numpy as np
from numba import cfunc, carray
# Note this script uses the absorbing boundaries extension installed with pipic
from pipic.extensions import absorbing_boundaries
import matplotlib.pyplot as plt
import os


# ==============================================================================
# SIMULATION SETUP
# ==============================================================================

```

```python
22  # Plasma parameters (CGS units)
23  # Temperature in units of [erg] (T=T_k * k_B, where T_k is temperature in Kelvin
24  # and k_B is the Boltzmann constant [erg/K])
25  temperature = 1e-6 * consts.electron_mass * consts.light_velocity**2
26  density = 1e18 # particle number density in units of [1/cm^3]
27  debye_length = np.sqrt(
28      temperature / (4 * np.pi * density * consts.electron_charge**2)
29  ) # in units of [cm]
30  plasma_period = np.sqrt(
31      np.pi * consts.electron_mass / (density * consts.electron_charge**2)
32  ) # in units of [s]
33
34  # Simulation box parameters
35  l = 128 * debye_length # simulation box length
36  xmin, xmax = -l / 2, l / 2
37  nx = 128 # number of cells
38  timestep = plasma_period / 64
39
40  # Electric field parameters
41  field_amplitude = (
42      0.01 * 4 * np.pi * (xmax - xmin) * consts.electron_charge * density
43  )
44  dmin, dmax = -l / 4, l / 4 # region to apply field
45
46  # Initialize simulation with energy-conserving solver
47  sim = pipic.init(solver="ec2", xmin=xmin, xmax=xmax, nx=nx)
48
49  # ==============================================================================
50  # INITIAL FIELD
51  # ==============================================================================
52  @cfunc(types.field_loop_callback)
53  def initial_field(ind, r, E, B, data_double, data_int):
54      """Applies a sinusoidal initial electric field in the region dmin < x < dmax."""
55      if dmin < r[0] < dmax:
56          E[0] = (
57              field_amplitude
58              * np.sin(4 * np.pi * r[0] / (xmax - xmin))
59              * np.exp(-r[0] ** 2 / (2 * (0.2 * l) ** 2))
60          )
61
62  # Apply initial field
63  sim.field_loop(handler=initial_field.address)
64
65  # ==============================================================================
66  # PARTICLES
67  # ==============================================================================
68  @cfunc(types.add_particles_callback)
69  def density_profile(r, data_double, data_int):
70      """Uniform density profile."""
71      return density
72
73  # Add particles according to density_profile
74  sim.add_particles(
75      name="particle_name", # name of the particle species
76      number=nx*100, # total number of particles to add
77      density=density_profile.address, # density profile function
78      charge=consts.electron_charge, # particle charge
79      mass=consts.electron_mass, # particle mass
80      temperature=temperature, # particle temperature
81  )
82
83  # ==============================================================================
84  # ABSORBING BOUNDARIES EXTENSION
```

22

```python
85   # ============================================================================
86   data_int = np.zeros((1,), dtype=np.intc) # used to pass iteration number
87   boundary_size = xmax / 2
88
89   sim.add_handler(
90       name=absorbing_boundaries.name,
91       subject="particle_name,cells", # apply to both particles and cells
92       # particle handler
93       handler=absorbing_boundaries.handler(
94           # pass address to cell and particle data
95           sim.ensemble_data(),
96           # pass address to simulation box geometry
97           sim.simulation_box(),
98           # pass adress to density profile function
99           density_profile=density_profile.address,
100          # size of boundary (in cm)
101          boundary_size=boundary_size,
102          # size of temperature of particles to be added
103          temperature=temperature,
104          # number of particles to be added per cell
105          particles_per_cell=100,
106      ),
107      field_handler=absorbing_boundaries.field_handler(
108          # pass address to simulation box geometry
109          sim.simulation_box(),
110          # pass size of time step
111          timestep=timestep
112      ),
113      # pass address to data_int for passing iteration number
114      # (see RUN SIMULATION section)
115      data_int=pipic.addressof(data_int),
116  )
117
118  # ============================================================================
119  # DIAGNOSTICS
120  # ============================================================================
121
122  # --- Field diagnostic ---
123  # array for saving Ex field
124  field_dd = np.zeros((nx,), dtype=np.double) # array for saving Ex field
125  # callback function for field diagnostic
126  @cfunc(types.field_loop_callback)
127  def field_callback(ind, r, E, B, data_double, data_int):
128      """Store Ex."""
129      data = carray(data_double, field_dd.shape, dtype=np.double)
130      data[ind[0]] = E[0]
131
132  # --- Particle phase space diagnostic ---
133  # array for saving particle (integrated) phase-space
134  particle_dd = np.zeros((64, nx), dtype=np.double)
135  # momentum range for phase space
136  pmin = -5 * np.sqrt(consts.electron_mass * temperature)
137  pmax = 5 * np.sqrt(consts.electron_mass * temperature)
138  # momentum and position steps
139  dp = (pmax - pmin) / particle_dd.shape[0]
140  dx = (xmax - xmin) / particle_dd.shape[1]
141  # callback function for particle phase space diagnostic
142  @cfunc(types.particle_loop_callback)
143  def particle_callback(r, p, w, id, data_double, data_int):
144      """Calculate particle momentum-position phase space density."""
145      data = carray(data_double, particle_dd.shape, dtype=np.double)
146      ip = int(particle_dd.shape[0] * (p[0] - pmin) / (pmax - pmin))
147      ix = int(particle_dd.shape[1] * (r[0] - xmin) / (xmax - xmin))
```

```python
148     if 0 <= ip < particle_dd.shape[0] and 0 <= ix < particle_dd.shape[1]:
149         data[ip, ix] += w[0] / (dx * dp)  # normalize
150
151 # ============================================================================
152 # PLOTTING SETUP
153 # ============================================================================
154 fig, ax = plt.subplots(2, 1, constrained_layout=True)
155
156 # Field plot
157 x_axis = np.linspace(xmin, xmax, nx)
158 Ex_plot = ax[1].plot(x_axis, field_dd)[0]
159 ax[1].set_ylim(field_amplitude, -field_amplitude)
160
161 # Phase space plot
162 xpx_plot = ax[0].imshow(
163     particle_dd,
164     extent=[xmin, xmax, pmin, pmax],
165     aspect="auto",
166     origin="lower",
167     cmap="YlOrBr",
168     vmin=0,
169     vmax=6 * density / (2 * pmax),
170     interpolation="none",
171 )
172
173 # Labels
174 ax[0].set_title("Plasma oscillations")
175 ax[1].set_xlabel("x (cm)")
176 ax[0].set_ylabel("$p_x$ (cm g/s)")
177 ax[1].set_ylabel("$E_x$ (StatV/cm)")
178
179 # ============================================================================
180 # RUN SIMULATION
181 # ============================================================================
182 simulation_steps = int(8 * plasma_period / timestep)
183 # Number of figures to save (every 8 steps)
184 figures = simulation_steps // 8
185 # Directory to save figures
186 save_to = "./output/"
187
188 # Create output directory
189 if not os.path.exists(save_to):
190     os.makedirs(save_to)
191
192 for i in range(figures):
193     # Update iteration counter for absorbing boundary extension
194     data_int[0] = i * 8
195
196     # Advance simulation (use_omp=True to enable OpenMP parallelization)
197     sim.advance(time_step=timestep, number_of_iterations=8, use_omp=True)
198
199     # Collect diagnostics
200     sim.field_loop(
201         handler=field_callback.address,
202         # pass address to field_dd array for storing Ex
203         data_double=pipic.addressof(field_dd),
204         # enable OpenMP parallelization
205         use_omp=True,
206     )
207     particle_dd.fill(0)
208     sim.particle_loop(
209         # name of particle species to be processed
210         name="particle_name",
```

24

```
211        handler=particle_callback.address,
212        # pass address to particle_dd array for storing phase space
213        data_double=pipic.addressof(particle_dd),
214    )
215
216    # Update plots
217    Ex_plot.set_ydata(field_dd)
218    xpx_plot.set_data(particle_dd)
219
220    # Save figure
221    plt.savefig(save_to + f"plasma_oscillation_{i:03d}.png", dpi=150)
```

B   Electrostatic solver

The following scripts provide an implementation of an electrostatic solver based on the predefined solver structure of π-PIC: `pic_solver` (see section B.1) and `field_solver` (see section B.2).

B.1   `ES1D_field_solver.h`

```
1  /*-------------------------------------------------------------------------------
2  This file is part of pi-PIC.
3  pi-PIC, Copyright 2023 Arkady Gonoskov
4  -------------------------------------------------------------------------------
5  pi-PIC is free software: you can redistribute it and/or modify it under the terms
6  of the GNU General Public License as published by the Free Software Foundation,
7  either version 3 of the License, or (at your option) any later version.
8
9  pi-PIC is distributed in the hope that it will be useful, but WITHOUT ANY
10 WARRANTY; without even the implied warranty of MERCHANTABILITY or FITNESS FOR A
11 PARTICULAR PURPOSE. See the GNU General Public License for more details.
12
13 You should have received a copy of the GNU General Public License along with
14 pi-PIC. If not, see <https://www.gnu.org/licenses/>.
15 -------------------------------------------------------------------------------
16 Website: https://github.com/hi-chi/pipic
17 Contact: arkady.gonoskov@gu.se
18 -------------------------------------------------------------------------------*/
19 // Description: Implementation of an electrostatic 1D solver.
20
21 #include "ensemble.h"
22 #include "ES1D_field_solver.h"
23
24 struct ES1DPicSolver: public pic_solver
25 {
26    double timeStep;
27    ES1DFieldSolver *field;
28
29    ES1DPicSolver(simulationBox box){
30        field = new ES1DFieldSolver(box);
31        Field = field;
32        Ensemble = new ensemble(Field->box);
33        name = "electrostatic_1d";
34    }
35    ~ES1DPicSolver(){
36        delete Ensemble;
37        delete field;
38    }
39
40    void advance(double _timeStep){
41        timeStep = _timeStep;
```

```cpp
            Ensemble->advance_singleLoop<ES1DPicSolver, ES1DFieldSolver>(this, timeStep);
    }

    void halfstep(particle &P, double charge, double mass, double timeStep){
        double3 E;
        double3 B;
        // get electric field at the particle position
        field->getEB(P.r, E, B);
        // pull back/move forward 1/2 timestep to initalize/remove leapfrog scheme
        P.p.x += timeStep*charge*E.x/2;
    }

    void preStep(double timeStep){
        for (int it = 0; it < int(Ensemble->type.size()); it++){
            for(ensemble::nonOmpIterator iP = Ensemble->begin(it); iP < Ensemble->end()
                ; iP++){
                particle *P = &*iP;
                // pull back momentum 1/2 timestep to initalize leapfrog scheme
                halfstep(*P, Ensemble->type[it].charge, Ensemble->type[it].mass, -
                    timeStep);
            }
        }
    }

    void preLoop()
    {
        field->advance(timeStep);
        for(size_t ix = 0; ix < field->Jx.size(); ix++){
            field->Jx[ix] = 0;
        }
    }

    void processParticle(particle &P, double charge, double mass, double timeStep){
        simulationBox &box(field->box);
        double3 E;
        double3 B;
        field->getEB(P.r, E, B); // get electric field at the particle position
        P.p.x += timeStep*charge*E.x; // advance particle momentum
        P.r.x += timeStep*P.p.x/(mass); // advance particle position
        double l = box.max.x - box.min.x;
        // periodic boundary conditions
        if (P.r.x < box.min.x) P.r.x += (box.max.x - box.min.x);
        else if (P.r.x > box.max.x) P.r.x += (-box.max.x + box.min.x);

        // deposit current
        int indx = int((P.r.x - box.min.x)/box.step.x);
        double w_left = field->CIC(P.r.x, indx, box.step.x, box.min.x);
        double w_right = 1 - w_left;

        field->Jx[indx] += w_left*P.w*charge*(P.p.x/mass)/box.step.x;
        field->Jx[(indx + 1) % box.n.x] += w_right*P.w*charge*(P.p.x/mass)/box.step.x;
    }

    void postStep(double timeStep){
        for (int it = 0; it < int(Ensemble->type.size()); it++){
            for(ensemble::nonOmpIterator iP = Ensemble->begin(it); iP < Ensemble->end()
                ; iP++){
                particle *P = &*iP;
                // move forward momentum 1/2 timestep to remove leapfrog scheme
                halfstep(*P, Ensemble->type[it].charge, Ensemble->type[it].mass,
                    timeStep);
            }
        }
```

```
101      }
102
103      // empty methods
104      void postLoop(){}
105      void startSubLoop(int3 i3, double charge, double mass, double timeStep){}
106      void endSubLoop(){}
107
108  };
```

B.2 `ES1D_pic_solver.h`

```
1   /*-------------------------------------------------------------------------------
2   This file is part of pi-PIC.
3   pi-PIC, Copyright 2023 Arkady Gonoskov
4   -------------------------------------------------------------------------------
5   pi-PIC is free software: you can redistribute it and/or modify it under the terms
6   of the GNU General Public License as published by the Free Software Foundation,
7   either version 3 of the License, or (at your option) any later version.
8
9   pi-PIC is distributed in the hope that it will be useful, but WITHOUT ANY
10  WARRANTY; without even the implied warranty of MERCHANTABILITY or FITNESS FOR A
11  PARTICULAR PURPOSE. See the GNU General Public License for more details.
12
13  You should have received a copy of the GNU General Public License along with
14  pi-PIC. If not, see <https://www.gnu.org/licenses/>.
15  -------------------------------------------------------------------------------
16  Website: https://github.com/hi-chi/pipic
17  Contact: arkady.gonoskov@gu.se
18  -------------------------------------------------------------------------------*/
19  // Description: Implementation of an electrostatic 1D solver.
20
21  #include "ensemble.h"
22  #include "ES1D_field_solver.h"
23
24  struct ES1DPicSolver: public pic_solver
25  {
26      double timeStep;
27      ES1DFieldSolver *field;
28
29      ES1DPicSolver(simulationBox box){
30          field = new ES1DFieldSolver(box);
31          Field = field;
32          Ensemble = new ensemble(Field->box);
33          name = "electrostatic_1d";
34      }
35      ~ES1DPicSolver(){
36          delete Ensemble;
37          delete field;
38      }
39
40      void advance(double _timeStep){
41          timeStep = _timeStep;
42          Ensemble->advance_singleLoop<ES1DPicSolver, ES1DFieldSolver>(this, timeStep);
43      }
44
45      void halfstep(particle &P, double charge, double mass, double timeStep){
46          double3 E;
47          double3 B;
48          field->getEB(P.r, E, B); // get electric field at the particle position
49          // pull back/move forward 1/2 timestep to initalize/remove leapfrog scheme
50          P.p.x += timeStep*charge*E.x/2;
```

```
51          }

53      void preStep(double timeStep){
54          for (int it = 0; it < int(Ensemble->type.size()); it++){
55              for(ensemble::nonOmpIterator iP = Ensemble->begin(it); iP < Ensemble->end()
                    ; iP++){
56                  particle *P = &*iP;
57                  // pull back momentum 1/2 timestep to initalize leapfrog scheme
58                  halfstep(*P, Ensemble->type[it].charge, Ensemble->type[it].mass, -
                        timeStep);
59              }
60          }
61      }

63      void preLoop()
64      {
65          field->advance(timeStep);
66          for(size_t ix = 0; ix < field->Jx.size(); ix++){
67              field->Jx[ix] = 0;
68          }
69      }

71      void processParticle(particle &P, double charge, double mass, double timeStep){
72          simulationBox &box(field->box);
73          double3 E;
74          double3 B;
75          field->getEB(P.r, E, B); // get electric field at the particle position
76          P.p.x += timeStep*charge*E.x; // advance particle momentum
77          P.r.x += timeStep*P.p.x/(mass); // advance particle position
78          double l = box.max.x - box.min.x;
79          if (P.r.x < box.min.x) P.r.x += (box.max.x - box.min.x); // periodic boundary
                conditions
80          // periodic boundary conditions
81          else if (P.r.x > box.max.x) P.r.x += (-box.max.x + box.min.x);
82          // note that the momentum is defined as momentum per particle not per
                macroparticle

84          // deposit current
85          int indx = int((P.r.x - box.min.x)/box.step.x);
86          double w_left = field->CIC(P.r.x, indx, box.step.x, box.min.x);
87          double w_right = 1 - w_left;

89          field->Jx[indx] += w_left*P.w*charge*(P.p.x/mass)/box.step.x;
90          field->Jx[(indx + 1) % box.n.x] += w_right*P.w*charge*(P.p.x/mass)/box.step.x;
91      }

93      void postStep(double timeStep){
94          for (int it = 0; it < int(Ensemble->type.size()); it++){
95              for(ensemble::nonOmpIterator iP = Ensemble->begin(it); iP < Ensemble->end()
                    ; iP++){
96                  particle *P = &*iP;
97                  // move forward momentum 1/2 timestep to remove leapfrog scheme
98                  halfstep(*P, Ensemble->type[it].charge, Ensemble->type[it].mass,
                        timeStep);
99              }
100         }
101     }



105     // empty methods
106     void postLoop(){}
107     void startSubLoop(int3 i3, double charge, double mass, double timeStep){}
```

```
108    void endSubLoop(){}
109
110
111 };
```